Thermal Monitoring for Condition Based Maintenance of an X-ray Generator

Plamen V. Petkov,^{a,†} **Anton Zyapkov,**^{a,*} **Nedislav Veselinov,**^{a} **Kaloyan Genkov,**^{a} **Dimitar Todorov**^{b} **and Nikolay Zografov**^{a,b}

^{a}*Faculty of Physics, Sofia University "St. Kliment Ohridski",*
5 James Bourchier Blvd, 1164 Sofia, Bulgaria

^{b}*Danlex EOOD Research center,*
430 Tsar Boris III Blvd, 1619 Sofia, Bulgaria

E-mail: pvpetkov@phys.uni-sofia.bg, azjapkov@uni-sofia.bg,
nveselinov@phys.uni-sofia.bg, kgenkov@uni-sofia.bg,
dimitar.todorov@danlex.bg, nikolay.zografov@danlex.bg

The modern Non-Intrusive Inspection Systems (NIIS) are the backbone of air transportation security. The commercial aviation is impossible without them. Real-time evaluation of the NIIS technical condition is critical for the airport operators. Most of the operated worldwide NIIS were designed before the Internet of Things (IoT) era, and they don't have the options to provide real-time monitoring of their operational status. The examined X-ray generator, one of the most common types, is equipped with a stationary anode X-ray tube, mounted on an HS 100100V (Smiths Heimann Gmbh). The X-ray tube is immersed in cooling oil bath and encapsulated in stainless steel hull. The set of installed sensors consists of contact sensor arrays combined with a distant infrared sensors system for mapping the outer surface X-ray generator temperature profile. Real-live operational conditions were simulated to study steady-state thermal characteristics. Two indicators for normal operation with sufficient conservatism were selected for suitable monitoring of the operability of X-ray generator: the maximal allowed oil volume expansion and maximal long-term temperature at the inner oil volume boundary. They were estimated by the reported in this paper analytical 1-D thermal model after measurement of the outer hull's surface temperature. As a results, we distinguished four modes of X-ray generator operation: (1): 'normal operation;' (2): 'slow degradation;' (3): 'faster degradation;' and (4): 'failure.' The maximal temperatures on the hull's outer surface were estimated for each mode as follows: (1): $10\dots51°C$, (2): $51\dots80°C$, (3): $80\dots87°C$. The failure can take place at temperatures above $87°C$. We found that the 'normal operation' mode could be extended up to $60°C$ due to oil thermal expansion.

---

*Speaker

†Corresponding author

1. Introduction

The modern Non-Intrusive Inspection Systems (NIIS) are complicated machines that rely on X-ray generation and provide detection capabilities, supported by state-of-the-art electronics, electro-mechanics, software algorithms and solutions. They are the backbone of air transportation security. Currently, the commercial aviation is impossible without NIIS. Thus, the adequate real-time evaluation of the NIIS technical condition is critical for any airport smooth operation. However, most of the NIIS operated worldwide are designed before the Internet of Things (IoT) era, and they don't have the capabilities to provide information in real-time about their technical status. A solution for condition-based and predictive maintenance, developing recently (Predictive Maintenance Tool for NIIS – PMT4NIIS), aims to provide an early warning for possible failures, based on predictive algorithms using machine learning and Artificial Intelligence (AI) technologies [1]. That solution relies strongly on the technical data collected from the NIIS itself, along with retrofitted sensors, designed to monitor different physical and environmental parameters [2].

The X-ray generator is a major component in the NIIS system and is an all-electric system. The performance of this system is relatively easily controlled by a few electrical parameters. There is enough research, related to the aging of the elemental base to predict changes in its condition. Therefore, our research activity is dedicated to the reliability of the entire system, which is determined by the most critical component inside the generator: X-ray tube (Figure 1). The tube is the main X-ray generating component that functions in severe thermal conditions under which its structural materials are subjected to severe stresses. It is the failures of the X-ray tube that are the most costly in the process of operating the equipment. Therefore, the efforts of the current analysis are dedicated to monitoring of the X-ray generator normal operation conditions and prediction the thermal status of its X-ray tube. Chapter two outlines specific issues, related to overall X-ray generator design. The developed experimental approach and its practical implementation are presented in chapter three. Here is given overall information about our thermal monitoring system, which includes contact thermometers, attached to the X-ray generator surface as well as infrared (IR) cameras (sensors), used for distant temperature monitoring. In the same chapter is reported study on the IR sensors signal attenuation depending on the distance from the measured surface. The experimental data and theoretical analysis are given in chapter four. The discussion of the results is provided in chapter five and finally the conclusions, based on the current study are given in chapter six.

2. X-ray generator working conditions and energy transfer paths

Figure 1 shows schematics of the X-ray tube, respectively. The electrons are generated by the tungsten wire (cathode in Figure 1, called emitter or filament), which is heated to a temperature above $2000°C$, with the maximum permissible temperature being limited to $2700°C$. If the voltage between the cathode and the anode is U, V and the current through the tube anode and cathode is I, A, then each electron will reach the anode with a kinetic energy of U, eV. The total energy deposited on the anode is $\omega U I t$, where ω is a wave weighting factor to account for the *rms* value of the generator voltage, [3]. The weighting factor is related to the X-ray generation mode and takes the values 0.71 for one and two-pulse generators, 0.96 for six-pulse generators and 0.99 for 9-pulse

generators, respectively, [4]. Practically, this is all the energy generated by the electronic circuit (X-ray generator) without taking into account the losses in the circuit itself. In the prototype, used in current analysis, the X-ray tube is developed by Svetlana-Rentgen [5] type No. 0,32BPM 25-160, design which is widely used.
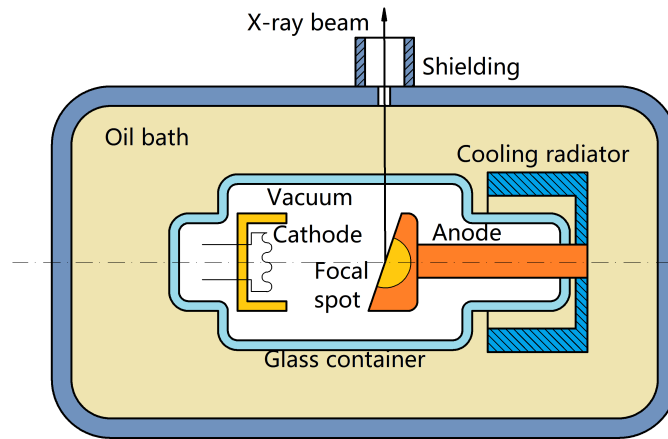
Figure 1: General outline of a X-ray generator

In general, the resulting X-rays takes only 1% of the released energy. The remaining 99% is released in the anode, made by pure copper after the electrons hit thetarget, a designated region, called focal spot, made by the implanted tungsten in the anode (see Figure 1). The generated X-rays depends mainly on the properties of the filament of the cathode, which in our case is made by tungsten and have a peak at about 60 MeV. The peak is characteristic to this material, [3]. The cathode potential difference (heating voltage) varies up to 4.2 V, and the heating current is up to 4.4 A DC. The electrons generated by the filament are accelerated under the action of a potential difference varying for different devices. For HS 100100V (HI-SCAN 6040 aX/aTiX) type systems, [6], it is around 160 kV. From the entire photon spectrum, only photons with energies from 50 to 70 keV are used for imaging, while the remaining ones are being absorbed by the biological shielding of the generator, made by lead, tightened to the outer surface of the hull by five belts (see Figure 3a). Since the photons carry a minimal amount of the released energy, it is not taken into account and ignored in the current model. In this case, it is very important to account for the heating of the focal spot target of the anode due to the deposited energy from the electron beam. The key characteristic factor of the X-ray generator "lifetime" is the temperature of the anode target. In the case of the current NIIS investigation, the melting temperature of the tungsten focal spot is $3410°C$. The entire system is placed in an oil bath, where the oil is designated to cool the system during normal operation (Figure 1). Therefore, the produced amount of heat undergoes dissipation in the oil bath in which the X-ray tube is immersed. This way, the X-ray tube is cooled. During the normal operation of the equipment, the "focal spot" can reach values up to $2500°C$. The maximum permissible temperature of its heating without damage is $2757°C$. The anode is made of copper (which melting temperature is about $1336°C$). Its temperature during the normal operation can reach up to $1000°C$. The energy, released in the focal spot is produced in the form of heat that further is transported from the anode to the cooling radiator, where it is removed by the oil to the outer surface of X-ray generator [8]. The X-ray generator is sealed, and no information could be obtained

of its cooling status during the normal operation. Therefore, the physical and chemical properties of the oil, used in X-ray generators should obey the strict requirements of several standards, listed in Refs. [8, 9, 10]: It must contain no water, water-soluble acids, alkali and particulate matter. The total acidity should be below 1.2 mgKOH/kg, [10]. The dielectric strength of this type of oil depends on the electrons accelerating voltage operation range. In the currently investigated machine, it is required to be within 40 kV to 65 kV, [8]. The temperature ranges of oil operation are deduced from the analysis, made in Refs. [9,10]: Normally, the oil should be operated within the range of 10 °C to 80 °C, [6,10]. In the range from 80 °C to 250 °C, for long term operation, stray gases (such as ethane and hydrogen) formation could be observed and finally $300°C$ is defined as operational limit, Ref. [10], which could vary depending of the dielectric oil boiling point.

This imaging system belongs to so called "fixed target X-ray generators" that are designed to operate in a relatively low power mode due to the temperature limitations imposed on the materials used, [7,4,3].

3. Experimental approach

In the present study, we propose a thermal monitoring approach as a new source of valuable data for estimating the X-ray generator's technical condition and input to the predictive models. The study provides both analytical and experimental data. The proposed analytical model has been extended with the experimental results, based on the large data-sets (big-data), collected by appropriate sensors.

The thermal parameters of the x-ray generator were studied during numerous long tests run series conducted on HS 100100V, located at the Danlex research center. This X-ray generator type is widely implemented on similar X-ray security inspection systems for luggage and cargo. To reach a steady state of the x-ray generator thermal status, most of the respective test runs have lasted more than 24 hours of continuous workload (X-ray beaming), simulating real operating conditions.

The experimental setup consists of contact sensor arrays combined with a distant infrared sensors system, in order to provide the temperature mapping of the hull's entire outer surface of the X-ray generator. These data are used for generation of boundary conditions for the thermal analytical model.

3.1 Installation of contact thermometers

The contact measurement of the X-ray generator surface temperature is performed by 35 digital temperature sensors of DS18B20 type (working in the range from $-55°$ to $125°$) with precision of $±0.5°C$. They were mounted in specially made wooden fixtures, whose purpose was to attach them securely to certain points on the hull's outer surface (see Figure 2a), [11]. The locations of the sensor fixtures were aligned with the parts of the volume of the hull of greatest interest to the research team. The distribution of sensors was performed as follows: Along the length of the X-ray axis, nine sensors were placed in a row (line), Figure 3a. An exception is the area around X-ray beam radiation flux shield: Because of the impossibility to place thermometers there, only five sensors were considered. This way, four lines are formed (see Figure 2a). Each line is assigned one letter of the Latin alphabet, starting from left to right. After the letter there is a number that indicates the cross-sectional position of the sensor. All equal numbers are aligned to form a X-ray generator

cross-section. During the mounting, there was avoided placing a sensor on the belts holding the X-ray generator's shield (see Figure 3a). The further measurement with IR sensors reveals that the temperature drops at these zones due to the improved cooling, see Figure 7. Separately, seven more

(a) Crossectional distribution of contact thermometers

(b) Determination of IR sensors optimal position
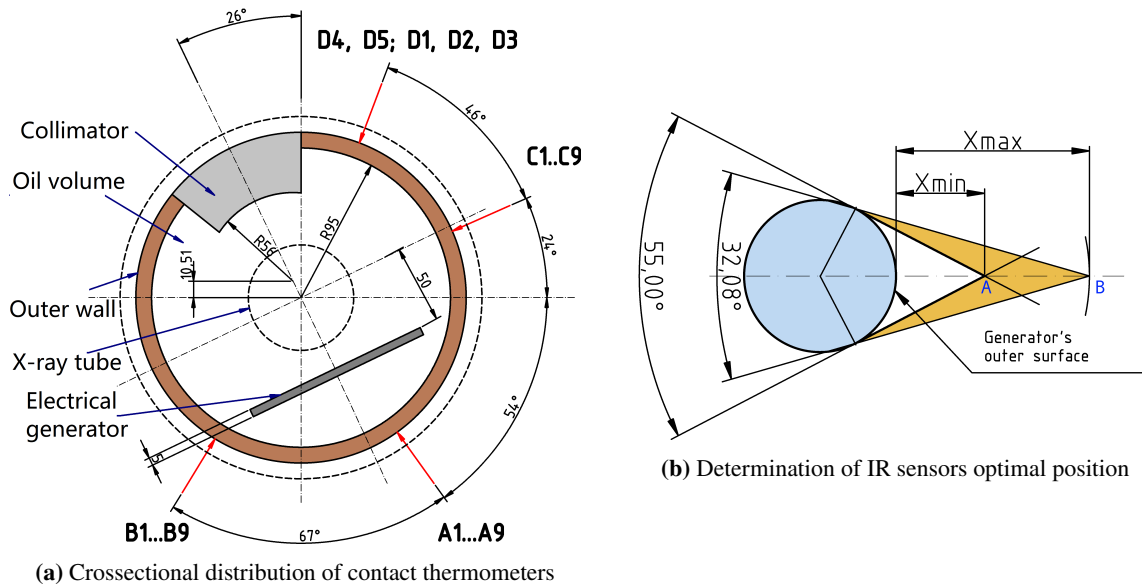
Figure 2: Schematic presentation of IR and contact thermometers mounting schemes

sensors in a series, denoted as T1...T7, were installed in the NIIS volume at various points of specific interest. They measure the temperature inside the body of the testing machine (HI-SCAN 6040 aX/aTiX). As a result, two sets of temperatures are formed in the NIIS housing, see Figure 3b: (a) temperatures in the immediate vicinity of the X-ray generator, T1...T5; (b) ambient, inside the machine temperatures, T6 and T7. Once the machine entered a stationary operating mode (NO, Figure 6), the temperature values became very stable and no significant difference between statistically measured temperatures by the two sets is detected. They exhibit little deviations in their nominal values at different external environmental conditions, around NIIS. Generally, it was found no significant variations in T1-T7 measurement (see Table 1) once the machine entered stationary mode of operation.

3.2 Infrared sensors characterization

After performance of the positional analysis of the available space in the HS 100100V machine, there were identified possible positions for mounting of IR sensors. We installed four tiny IR cameras, MLX90640 — BA with silicon made lens and thermopile array sensors. Further in the text, we designate to them numbers from S1 to S4. The 32×24 px. array sensor uses a $100\,\mu$m pixel technology. It offers very good performance for applications that do not require images with high-resolution or a high rate of frames, which means that they cannot provide reliable results in transient conditions. Silicon optics is operating in the $1.2\,\mu$m to $7\,\mu$m wavelength range. The lenses are mounted such a way to guarantee Field of View (FOV) 55° [12,13]. According to the specification, their operational range is from $-40\,°$C to $200\,°$C with precision of $\pm 2.0\,°C$. The resolution of their matrix is 32×24 px., [12]. Image detection angle varies from $32\,°$ to $55\,°$

and it is established according to the IR sensors characteristics and the X-ray machine capabilities to support a suitable structure for sensors holding, [12]. The optimal distance for their position is identified to lie between the points AB in Figure 2b. Using the software LibreCad, [14], an analysis was performed for evaluation of the possible positions of the infrared sensors in which the resolution angle of 55° is ensured. Geometrically, there was found that optimal distance varies between x_{min} = 64 mm and x_{max} = 140 mm. Figure 2b shows our preliminary geometric study to determine the optimal position of the sensors. It can be seen that if placed 140 mm normally to the surface of the generator at position B, (x_{max}) , the infrared camera will cover a range from 140 mm to 176 mm due to the surface curvature. In the second position A, the distance to the sensors will vary from 64 mm to 106 mm, see Figure 2b. If the IR camera (sensor) is very close to the surface, it will cover a smaller part from the outer the X-ray generator hull's surface and part of the environment, which will lead to a potential degradation of the measurement accuracy, [12]. As the distance from the X-ray generator increases, the IR cameras resolution decreases and the temperature readings may significantly deviate from the real values (see further in the text). After IR sensors installed at the selected positions around X-ray generator, the emissivity was selected also 0.95, according to the measured surface of X-ray generator and the vendor specifications. The

(a) Picture with contact thermometers distribution at X-ray generator surface. In the picture are seen sensors $C1 \ldots C9$ and $D4, D5, D1 \ldots D3$.
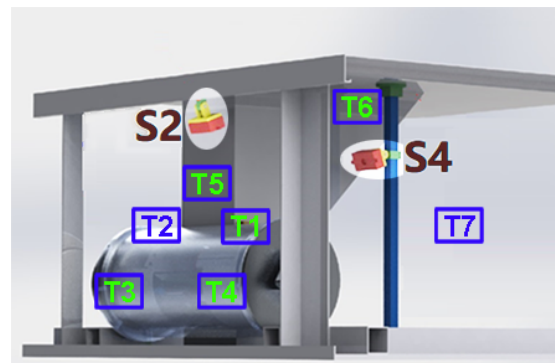
(b) Positional placement of IR sensors. In the picture are seen the sensors S2 and S4. The two others are positioned symmetrically to them on the other side of X-ray generator

Figure 3: Schematic presentation of IR and contact thermometers installation.

assessment of the resolution of the IR sensors was carried out as follows: In laboratory conditions, a hot-tip solder was placed in front of the camera at various fixed distances, see Figure 4 and Figure 5. The obtained sequence of images is used further for determination of the spatial sensitivity of the IR sensors. The results show a decrease of the camera resolution with an increase of the distance. Based on the measurements at different distances, an empirical relation was found for prediction of the measured surface temperature with accounting the signal attenuation (Figure 5), as follows:

$$T_{max} = A \ln x + B \tag{1}$$

Where A and B are empirical constants, characterizing the particular temperature field. The attenuation effect of the entire measurement channel follows logarithmic law. For temperatures up to 110 °C, we obtained: $A = -22.95$ and $B = 152.73$ where the distance is given in cm. Further
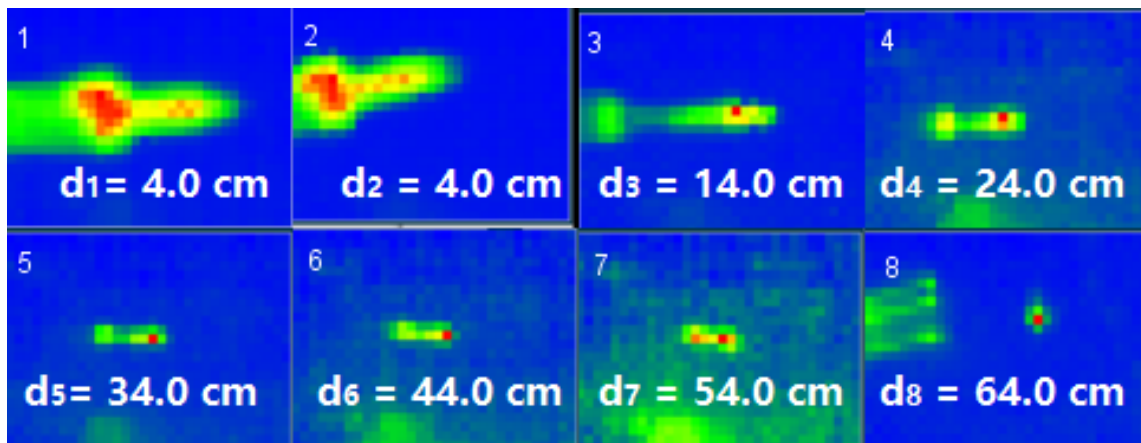
Figure 4: Detected temperature by IR sensors at different distances, where $d_1 \ldots d_8$ denote distances from the hot-tip solder

investigation indicate that for lower temperatures, not using Equation 1 for surface temperature restoring will bring little distortion of te measurement accuracy. At a distance greater than 20 cm,
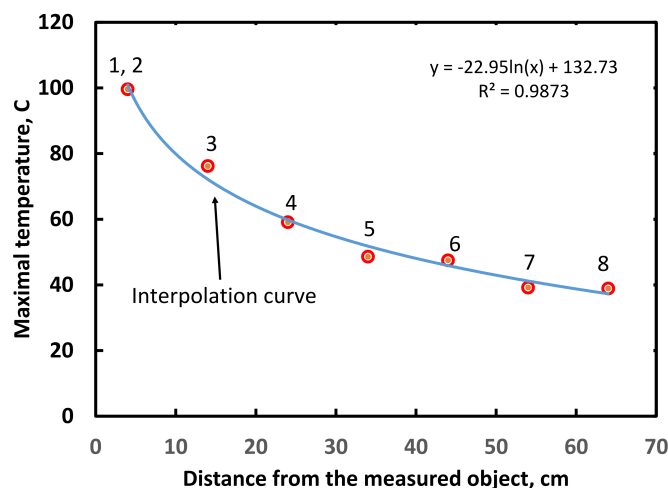
Figure 5: Measured constant temperature by IR sensors at different distances (note that numbers in the figure correspond to the numbers in Figure 4)

the measured temperature is hardly distinguished from the background temperature. The optimal measurement distance is determined to be about 14 cm from the observed object.

From Figure 3b is seen that due to the limited space, there cannot be installed IR cameras pointing to the surface of the X-ray generator from the the X-ray machine outer edge (the side of contact sensors $C1 \ldots C9$, Figure 3a). The X-ray beam and its shielding also divide the generator housing in two distinguished parts suitable for optical observation, Figure 3. For these reasons, four cameras were installed at the inner side of the generator to cover its surfaces pointing inside the X-ray machine. Each IR camera is numbered. In Figure 3b, there are shown only IR cameras S2 and S4. The other two IR cameras are placed symmetrically on the other side of X-ray generator, noted correspondingly S3 and S1. All IR sensors were mounted at 140 mm from generator surface

to avoid distorted data from the pixels at the IR cameras edges, because of the lower precision $\pm 3.0°C$, as specified b the vendor, [12]. With calibration sets, developed for the purpose of the analysis, we found that the distance between two pixels is v:h = 8:6 mm in average. Further, during the measurement from S1 and S4 we could not obtain reliable data and it was found that only results from S2 and S3 are sufficient to provide information about the temperature field at the inner X-ray generator surface.

4. Analytical solution

During the operation of X-ray machine, the following three modes can be distinguished: start-up procedure (SU), normal operation (NO) and shut-down (SD) modes, (see Figure 6). Two of the regimes (SU and SD) are non-stationary and a change as a function of the time of the measured temperature values is denoted. Since the most important for long term operation are stationary modes (NO), the investigation is limited to study only of these regimes. In this case, the system is fully loaded. Therefore, as the time independence of measured temperatures takes place, the statistical approach is suitable for further data analysis. Figure 7 shows the typical loading scheme of the testing machine at the Danlex research center, that imitates the real loading at the airport operation. Two sets of regimes are shown: SU-1, NO-1, SD-1 which continues longer in the time and shorter: SU-2, NO-2, SD-2. After the statistical analysis performance of all NO regimes, no significant deviation in estimated outer hull's (boundary) surface temperatures is obtained. It also was found that these temperatures maintain the same stable average values at different environmental condition. Note that in Figure 6 the maximal steady state values of outer surface temperature do not exceed $49.8 \pm 5.5°C$ Although there could be developed analytically solvable theoretical model in three dimensions involving heat conduction and convection heat transfer, practical problems, related to the suitable description of the temperature field inside the generator for the purpose of PMT4NIIS arise. Because of this, an one-dimensional model for heat conduction, for finding the distribution of the temperature field inside the oil volume in two dimensions, was implemented (see Equation 2). Such assumption is not entirely correct, because inside the volume not only heat conduction but also convective heat transfer takes place, [15]. However, based on the results, published in [16], the heat conduction model can be extended with an effective heat conduction coefficient, λ_{eff} which accounts not only the conductive but also the convective part of the heat removal process, [17]. Further, we propose the usage two-layer model, where outer X-ray generator stainless steel huff (outer shell) holds the inner oil volume, that fills the entire space, surrounding X-ray tube. At the center of these cylinders is assumed an inner heated cylindrical surface, T_i, as seen in Figure 8. For simplicity, we assume that the diameter of this surface is equal to the X-ray tube outer diameter, because (as mentioned in section 2), it is considered to be the most critical component for the X-ray generator operation.
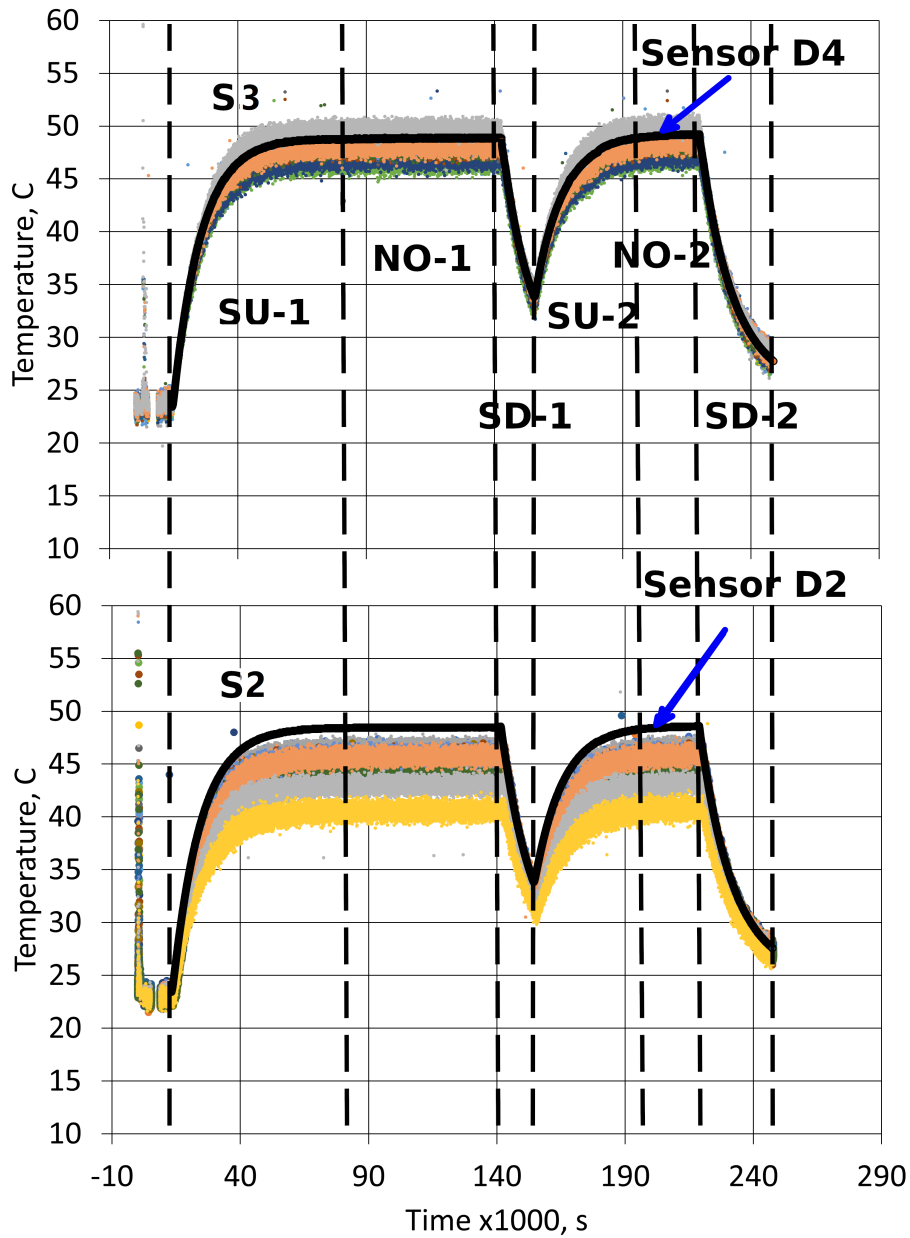
Figure 6: Three modes differentiated during the operation of X-ray machine: startup (SU), normal operation(NO), shutdown (SD). The plot presents two full operations 1:SU-NO-SD, 2:SU-NO-SD. The obtained data from IR sensors are compared with the nearest to them contact sensors: correspondingly D4 with S3 and D2 with S2

9

(a) Obtained data from sensor S2.

(b) Obtained data from sensor S3.
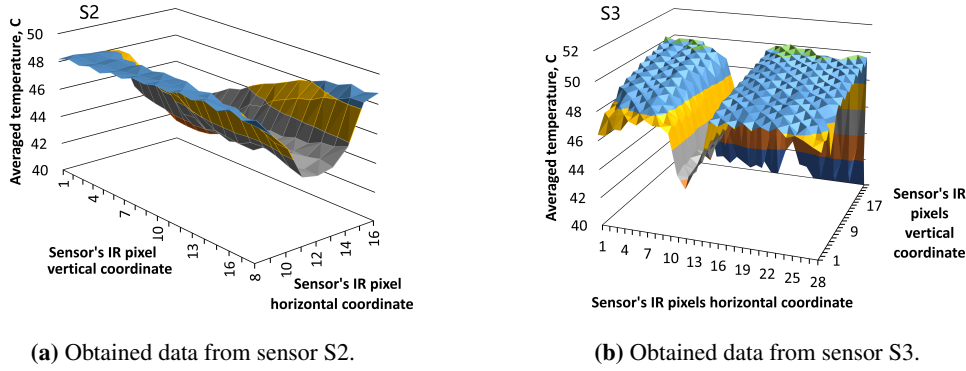
Figure 7: Three dimensional representation of measured temperature at the X-ray generator outer surface. Note the temperature falls due to improved cooling at the holding shields belts

4.1 Formulation of the equations

Based on the assumptions, presented above, the equation for heat conduction for stationary case is applicable as follows:

$$r\frac{d^2T}{dr^2} + \frac{dT}{dr} = 0 \tag{2a}$$

$$\frac{1}{r}\frac{d}{dr}\left[r\bar{\lambda}_o\left(\phi,r\right)\frac{dT}{dr}\right] = 0 \tag{2b}$$

where $\bar{\lambda}_o\left(\phi,r\right) \equiv \lambda_{eff}$ is the effective heat transfer coefficient that in general is not constant (ϕ and r are correspondingly angular and radial coordinates). However, for simplicity and due to the fact that temperature gradient during normal operation are not very high, we can assume it constant and denote further as λ_0. Therefore, Equation 2a describes stainless steel wall stationary heat transfer, while Equation 2b represents the oil volume heat transfer.

4.2 Boundary conditions

The boundary conditions at the outer surface of the X-ray generator wall are defined as follows: The first condition, Equation 3a describes the temperature at the surface, which is expected to be measured by contact thermometers and IR sensors, while the second Equation 3b is estimating the heat transfer governed by the temperature difference between the surface and the surrounding air.

$$T_{out}|_{r_w-\delta} = T_{out}|_{r_w+\delta} \equiv f(s) \tag{3a}$$

$$-\lambda_w\left.\frac{dT}{dr}\right|_{r_w-\delta} = \alpha_{out}(T_{out} - \bar{T}_{air}) = \alpha_{out}(f(s) - \bar{T}_{air}) \tag{3b}$$

where $T_{out} = f(s)$ indicates the surface temperature, obtained by the measurement system. The internal boundary conditions represent the temperature continuity at the oil/stainless steel boundary,
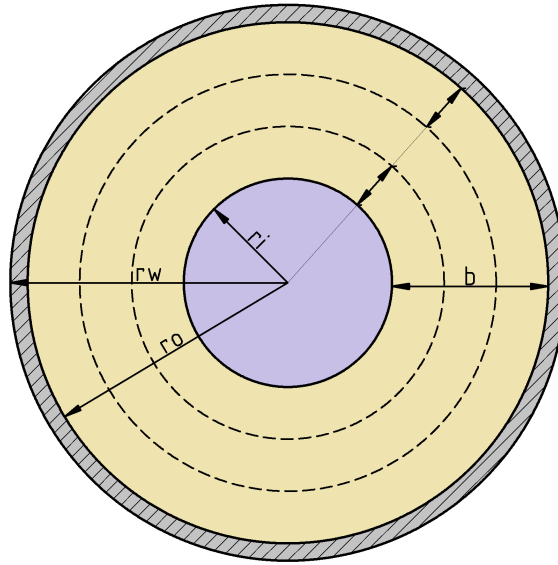
Figure 8: Schematic presentation of the modelling zone crosseton, where r_i is the assumed outer radius of X-ray tube, equal to the anode radius; r_o is the internal radius of stainless steel hull; r_w is the outer radius of X-ray generator.

Equation 3b as well as the heat flux transfer, Equation 4b:

$$T_o|_{r_o-\delta} = T_w|_{r_o+\delta} \tag{4a}$$

$$-\lambda_o \left.\frac{dT}{dr}\right|_{r_o-\delta} = -\lambda_w \left.\frac{dT}{dr}\right|_{r_o-\delta} \tag{4b}$$

In order to calculate correctly the boundary conditions, it is necessary to know the coefficient of heat transfer from the wall to the environmental air. Its determination is very difficult and is based mostly on empirical relations. In our case, the most suitably is to use the Nusselt number: $Nu = \frac{2r_w \alpha_{out}}{\lambda_w}$, where $2r_w$ is the outer diameter of the horizontal cylinder and the other quantities are explained in Table 1. For horizontal cylinder, the following relation can be used in cases of operation: $Nu = 0.481 + 0.172 \times \exp\frac{-0.258W}{2r_w} \times Ra^{0.2}$, where W is the length of the horizontal cylinder. The number $Ra = \frac{g\beta(T_{out}-T_{air})\, 8r_w^3}{v^2}Pr$ is the Raleigh number. For the air are valid the following data: compressibility is $\beta = 3.25 \times 10^{-3}$, kinematic viscosity is $v = 16.5 \times 10^{-6}\text{m}^2\,\text{s}^{-1}$, $Pr = 0.7$. [18][19]. During the normal operation (NO), the regime is very stable, then the applied constant value for heat transfer coefficient is given in Table 1.

4.3 Solution of the equations

The provided Equation 2 can be solved analytically for the given boundary conditions. Therefore, the solution is obtained for the solid wall region:

$$T = \left\{\frac{r_o \alpha_{out}}{\lambda_w}\left[f(s) - \bar{T}_{air}\right]\right\}\ln\frac{r_o}{r} + f(s) \tag{5}$$

11

Parameter	Description	Value
λ_o, [W m^{-1} K^{-1}]	Oil heat transfer coefficient	0.3714
λ_w, [W m^{-1} K^{-1}]	Wall heat transfer coefficient	52.0000
$\bar{T}_{air}$, [K($^\circ C$)]	Air bulk temperature	318(45)
r_w, [mm]	Internal wall radius	95.00
r_{out}, [mm]	Outer wall radius	105.00
r_i, [mm]	Equivalent X-ray tube outer radius (anode)	10.00
a_{out}, [W m^{-2} K^{-1}]	wall outer air heat transfer coefficient	7.9000

Table 1: The main parameters description and the assigned values used in calculations

The solution for the equation in the oil region is:

$$T = \left\{ \frac{r_o \alpha_{out}}{\lambda_o} \left[f(s) - \bar{T}_{air} \right] \right\} \ln \frac{r_w}{r} + \left\{ \frac{r_o \alpha_{out}}{\lambda_w} \left[f(s) - \bar{T}_{air} \right] \right\} \ln \frac{r_o}{r_w} + f(s) \tag{6}$$

Equation 5 and Equation 6, are suitable for the finding of the temperature field at the desired X-ray generator crossection. The heating source is at the inner boundary with radius r_i, with value defined in Table 1. It is assumed to be equal to the radius of X-ray tube anode (see Figure 8).

5. Data analysis and discussion

Although the analytical solution was obtained, the following problems arose, related to the practical implementation: (1) The IR cameras can not capture the full temperature field of the outer surface. This happened due to the limited space available in the test machine that we used (this possibly could be a general problem). (2) Contact thermometers are quite limited in number. In this particular case interpolation of the resulting values is necessary in order to be generated the temperature field at the surface. Given these two factors, the proposed two-layer one dimensional analytical model, applied along axial direction to each cross-section, proved itself to be suitable tool for thermal analysis of X-ray generator body.

The steady-state equation was defined in a cylindrical geometry, because the generator itself is a horizontal cylinder (Figure 3a), where the oil volume forms an annulus with heated inner surface, Figure 8. Two characteristics can be indicators for operational conditions of X-ray generator: the internal oil temperature in the vicinity of the X-ray tube and the oil density. As a result from theoretical analysis, two possible safety margins are identified: the temperature at the inner oil volume contacting X-ray tube surface and the oil volume thermal expansion. Figure 9a shows a diagram, obtained after the solution of Equation 5 and Equation 6 for the temperature field of the X-ray generator. Here, on the *x*-axis is positioned the X-ray generator surface temperature values as independent variable. Values obtained by the measurements (and further interpolation) can be selected there. After solution of Equation 2 with appropriate boundary temperature range 40 °C to 130 °C and linear dependence is found (marked in red in Figure 9a. In this figure, the corresponding temperature at the inner oil boundary (or the outer boundary of the X-ray tube) is found at the *y*-axis along the known line and obtained from solution of Equation 2). Based on the review, presented in section 2, four modes of operation of X-ray generator are distinguished:
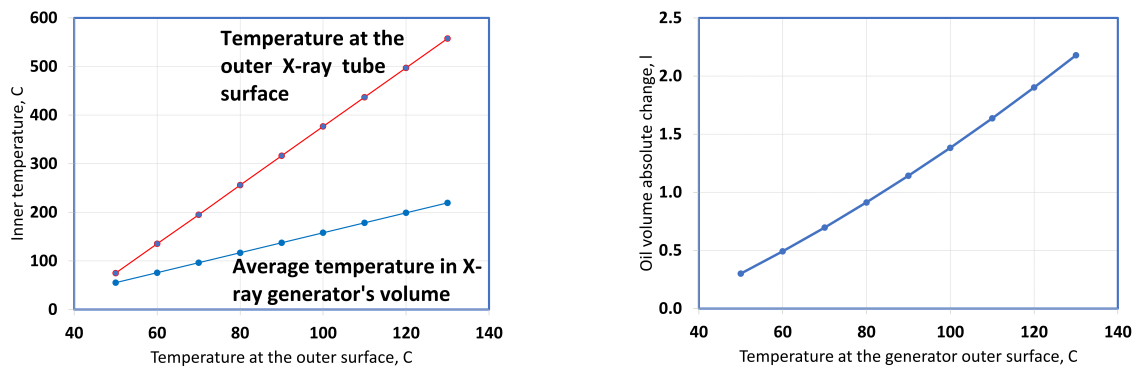
(a) Temperature profile on the outer X-ray tube wall and the average oil volume temperature related to the outer hull's surface temperature

(b) The volume of oil change, depending on the outer hull's surface temperature (the curve represents the average oil volume temperature)

Figure 9: Thermal characterization of X-ray generator operational steady-state condition.

Mode	Operational regime	Defined temperature range at X-ray tube cooling radiator	Measurable hull's outer surface temperature
1	Normal operation	$10°C \leq T_i < 80°C$	$10°C \leq T_{out} < 51°C$
2	Slow degradation	$80°C \leq T_i < 250°C$	$51°C \leq T_{out} < 80°C$
3	Faster degradation	$250°C \leq T_i < 300°C$	$80°C \leq T_{out} < 87°C$
4	Failure	$T_i > 300°C$	$T_{out} > 87°C$

Table 2: Relation between operational modes and temperatures

(1): 'normal operation;' (2): 'slow degradation;' (3): 'faster degradation;' and (4): 'failure.' The corresponding temperature ranges at the hottest surface of X-ray tube and calculated by Equation 2 possible values measured on the hull's outer surface are given in Table 2. The maximal temperature around the X-ray tube of $300°C$ corresponds to a temperature of $87°C$ on the outer surface of the hull's wall.

Similarly, the blue line in Figure 9a represents the average oil temperature, that further can be used for analysis of the oil expansion. Data obtained from [20] is used in the further analysis to obtain the volume change ΔV regarding STP conditions:

$$\Delta V = V_0 \beta \Delta T \tag{7}$$

where V_0 is the initial volume (at $20°C$), β is the compressibility of the oil, defined by $\beta = 5 \times 10^{-07} T + 0.0007$ for a given temperature T, K; ΔT is the temperature difference. It is known that the oil volume is expanded and the expanded fluid goes into the X-ray generator expansion cuff. It takes normally about 300–500 ml. oil, which in normal operation corresponds up to about $60°C$ at the outer hull' wall that slightly exceeds the limit for normal operation in Table 2.

6. Summary and Conclusions

The complete outer surface temperature profile of the X-ray generator was obtained using a combination of installed contact thermometers and distant infrared (IR) sensors. The measurements by infrared sensors were successfully verified with data from contact thermometers.

The obtained data from all measurements were used for generation of boundary conditions for the analytical model, reported in this paper. As a solution of Equation 5 and Equation 6, we obtained the temperature at the outer surface of X-ray tube cooling radiator, see Figure 1.

The solution of Equation 5 and Equation 6 reveals two major indicators of X-ray generator failures: the cooling oil density and the temperature at the inner surface of the oil volume annulus (outer surface of X-ray tube). The obtained results for normal operation by the two indicators fully agree, where the hull's outer surface temperature could be extended to $60°C$, see Equation 7, because of the oil thermal expansion. However, with the increasing of the temperature beyond the normal operation, slow chemical degradation of oil, straw gases production and worsening of heat removal could take place. Reaching the temperature of oil boiling at the outer X-ray tube indicates failure of the system which should take place at the hull's outer temperature of $87°C$, see Table 2.

Acknowledgements

References

[1] G. Nalbantov, D. Todorov, N Zografov, S. Georgiev, N. Bojilova *Predictive Maintenance Tool for Non-Intrusive Inspection Systems arXiv* (2021) (03 March 2021)

[2] N. Zografov *Method and system for predicting a failure probability of acomponent of an X-ray system EPO* **EP 20190781 A 20200812** (2021)

[3] D. R. Dance, S. Christofides, A. D. A. Maidment, I. D. McLea *Diagnostic Radiology Physics: A Handbook for Teachers and Students* Vienna, 2014

[4] P. Sprawls *The Physical Principles of Medical Imaging* 2-nd Ed, Medison: Medical Physics Pub, 1995

[5] Svetlana-Rentgen *Svetlana X-Ray* 2010 (Accessed May 21, 2021), 2022

[6] Smith Detection *HI-SCAN 6040 aX/aTiX and 7555 aX/aTiX* Smith, 2011

[7] D. E. Grideri, A. Wright, P. K. Ausburn, *Electron beam melting in microfocus x-ray tubes J. Phys. D: Appl. Phys.* **19**(1986) 2281-2292

[8] B. Pahlavanpour, M. Eklund, K. Sundkvist, *Revised IEC standard for maintenance of in-service insulating oil* Weidmann ACTI,Sacramento, CA, USA, 2004

[9] A. Nanfak, S. Eke, Ch. Hubert Kom, R. Mouangue, I. Fofana, *Interpreting dissolved gases in transformer oil: A new method based on the analysis of labelled fault data* IET Gener. Transm. Distrib. **23** 2 (2021) 873-880

[10] D. M. Mehta, P. Kundu, A. Chowdhury, P. Kundu, A. Chowdhury, *A Review on Critical Evaluation of Natural Ester vis-a-vis Mineral Oil Insulating Liquid for Use in Transformers: Part 1* IEEE Trans. Dielectr. Electr. Insul. **15** 21 (2016) 3032-3047

[11] Analog Devices (Dallas Semiconductor) *DS18B20 Programmable Resolution 1-Wire Digital Thermometer* (Accessed, December 15, 2022), 2022

[12] MELEXIS *MLX90640 32x24 IR array, Datasheet* 3901090640, (Accessed, December 01, 2021), 5 December 2019

[13] System Plus Consulting, *"Melexis Far Infrared Thermal Sensor MLX90640" Reverse Costing – Structure, Process & Cost Report* (Accessed, April 17, 2023), June 2019

[14] Wikipedia contributors *LibreCAD* In Wikipedia, The Free Encyclopedia (Retrieved, December 14, 2022), 2022

[15] M. Bottaro, M. Moralles, V. Viana, G. L. Donatiello, P. Silva *A practical method to determine the heating and cooling curves of x-ray tube assemblies J. Med. Phys.* **34** 10 (2007) 3982-3986

[16] G. D. Raithby and K. G. T. Hollands *A General Method of Obtaining Approximate Solutions to Laminar and Turbulent Free Convection Problems Adv. Heat Transfer* **11** (1975) 265-315

[17] A. F. Mills *Heat Transfer* Boston, Irwin Inc., 1992.

[18] F. Karim, B. Farouk and I. Namer *Natural Convection Heat Transfer from a Horizontal Cylinder between Vertical Confining Adiabatic Walls Trans. ASME J. Heat Transf.* **108** (1986) 291-298

[19] J. T. Cieslinski, S. Smolen, D. Sawicka *Free Convection Heat Transfer from Horizontal Cylinders Energies* **14** 3 (2021) 559

[20] E. I. Kazantcev *Industrial furnaces (Promishlennie pechi)* Handbook, 2nd edition, Metallurgy, Moscow 1975